Available online at www.sciencedirect.com
SCIENCE DIRECT®
Building and Environment 40 (2005) 589–600
BUILDING AND ENVIRONMENT
www.elsevier.com/locate/buildenv

Air flow characteristics of a room with square cone diffusers

Ying Sun, Theodore F. Smith*

Department of Mechanical and Industrial Engineering, The University of Iowa, Iowa City, IA 52242, USA

Received 18 November 2003; received in revised form 28 June 2004; accepted 9 July 2004

Abstract

A computational fluid dynamics model with radiant exchange between surfaces is developed to examine the air flow characteristics of a room with square cone diffusers. As an input to the full-scale 3-D room model, a 2-D diffuser model that supplies direction and magnitude of air flow into the room is developed and evaluated using infrared visualization. The room air flow model is assessed using several previously documented problems with various geometries and boundary conditions. Simulations are conducted for heating and cooling of the room with one or two supply air diffusers. The results show that the offset and lips of the diffuser work together to determine the discharge air angles, which play an important role in determining the room air flow patterns. For a certain discharge angle in the heating case, the air flows along the ceiling. The results indicate that, for the same supply air flow, operating only a single diffuser initiates more mixing of the room air flow, which results in enhanced temperature uniformity compared to that for two diffusers. Radiant exchange between the exterior window and interior surfaces causes a significant change in the window temperature.

Keywords: CFD simulation; Room air flow; Diffuser modeling; Air flow visualization

1. Introduction

The air flow pattern and temperature distribution within a room play important roles in determining the quality of the indoor environment and the amount of energy needed to condition the air for the room. Recent advances in computational fluid dynamics (CFD) and computer technology have provided powerful tools to predict air flow characteristics within a room that would almost be impossible to evaluate using experimental procedures. When using a CFD simulation, the reliability and accuracy of results depend on several factors, such as the turbulence model, the numerical scheme, and the modeling of the boundary conditions [1]. The supply air boundary condition is a crucial input because the momentum from the supply air diffuser dominates the room air flow. Due to the fact that most diffusers are much smaller compared to the size of the room, a CFD model that combines both the diffuser and the room would require significantly different length scales in CFD modeling and would require a large number of grid points to resolve the air flow at the diffuser outlet. To overcome theses factors, separate CFD models for the diffuser and room are developed and the appropriate modeling of the supply air boundary condition for a room becomes a challenge.

Several studies have focused on developing diffuser models to improve the representations of boundary conditions for CFD simulations in a room. Previous efforts on modeling diffusers include momentum modeling at and in front of the air supply devices. Heikkinen [2] replaced a complex diffuser with a model that has one or more rectangular slots and the same effective flow area as that for the complex diffuser. The model provided representative predictions for certain air flow patterns but had poor performance for non-isothermal applications. Chen and Moser [3] developed the momentum method, where the initial jet moment from

*Corresponding author. Tel.: +1-319-335-5680; fax: +1-319-335-5669.
E-mail address: tfsmith@engineering.uiowa.edu (T.F. Smith).

0360-1323/$ - see front matter © 2004 Elsevier Ltd. All rights reserved.
doi:10.1016/j.buildenv.2004.07.018

the diffuser is imposed as a boundary condition for the room model. The momentum method decouples the momentum and mass conditions to provide accurate air flows; however, implementation of this method in commercial CFD packages may be difficult. Djunaedy and Cheong [4] combined the diffuser jet characteristic equations with the method proposed by Heikkinen [2] to study the air flow from square cone diffusers. For the momentum modeling in front of the diffuser, Nielsen [5] proposed the box method that uses an imaginary box surface around the diffuser to represent the inlet boundary conditions. Srebric and Chen [6] applied both the box and momentum methods to study eight different commonly used diffusers, such as slotted and square cone types. The results showed good agreement with experimental measurements. Several cited methods for describing the air flow from diffusers are based on simplified inlet air flow models and rely on a limited number of measurements to identify the temperature and velocity of the air flow on surfaces that represent the diffuser.

Although the air flow can be laminar or weakly turbulent in some regions of a room, the overall flow features are often considered as turbulent [1]. The two-equation $k-\varepsilon$ model [7] is often used to describe turbulence for air flow in a room. The effect of buoyancy has been included in most models for room air flow [8,9]. Besides the typical convective and diffusive heat transfer, the radiant heat exchange between surfaces within a room is also accounted for in some studies; for example, Gan and Awbi [10] used view factors to evaluate the radiant heat exchange between room surfaces. As for boundary conditions, some CFD studies [11–13] assume that the supply air flow has uniform velocity and temperature at the inlet, which results in CFD predictions that may not be representative of actual air flow conditions.

Several investigations have been made to visualize the air flow around supply air diffusers. Zhao et al. [14] applied particle image velocimetry technique to measure the two-dimensional (2-D) air velocities in a full-scale room with a slot air inlet and a slot air outlet. Cehlin et al. [15] measured air temperatures close to a low-velocity diffuser for displacement ventilation using an infrared camera and a screen parallel to the supply air stream. These measurements provided data to validate CFD simulations.

The literature review indicates that a study that considers the diffuser modeling together with the room model to focus on the characteristics of the room air flow is needed. The objective of the present study is to examine the air flow pattern and temperature distribution in a room using CFD methodology. In this study, a model of the diffuser is constructed to determine the flow rate and direction of the air leaving a diffuser. The predictions from the diffuser model are compared to results using infrared thermography taken from a test facility with commercial building characteristics. A room air flow model is developed to use the outputs of the diffuser model as the input boundary conditions. The room model includes a turbulence model and considers buoyancy effects and radiation exchange. The topics of interest include the effects of (1) diffuser characteristics, (2) conditions of the entering air, and (3) radiation exchange on the air flow and temperature patterns within a room.

2. Model Development

2.1. System configuration

The air flow model of the room is developed based on the conditions that exist for the East-A Room of the Iowa Energy Center [16]. The room has conditions and configurations similar to those found in a commercial office; hence, the results reported are expected to have a wider range of application. Results from the simulations are intended to help in development of a simulation model for the room to be used for the purpose of examining control strategies and to provide guidance regarding how the indoor air quality requirements within the room are maintained.

The room shown in Fig. 1 has a length, X, of 5.49 m, a width, Y, of 4.57 m, and a height, Z, of 2.59 m. The exterior window with a height of 1.68 m occupies the upper portion of the exterior east-facing wall. The lower portion of the east wall contains three opaque sections. The outer two sections have a height of 0.91 m, a length of 1.16 m, and a ledge of a width of 0.30 m. The center section has a length of 2.25 m. All other surfaces of the room are interior surfaces. There are two $0.61 \times 0.61\ \mathrm{m}^2$ supply air diffusers centered in the ceiling and separated by 1.52 m. The return air diffuser is centered along the south edge of the ceiling. The diagonal wall at 45° is located 1.37 m away from the northwest corner and the door faces west.

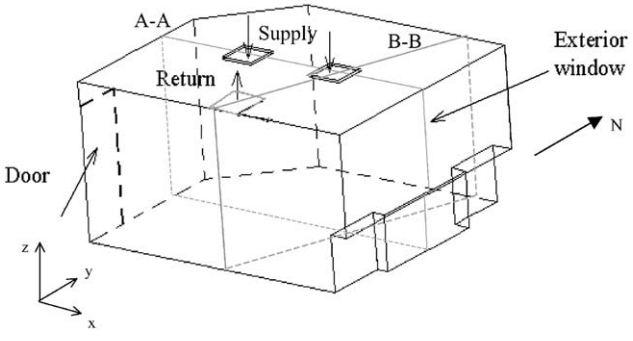

Fig. 1. Room model.

To determine the air flow characteristics of the room, two dimensionless numbers are examined. The Reynolds number based on an expected supply air inlet flow and a characteristic length defined using $\sqrt[3]{XYZ}$ indicates that the room air flow is in the transition regime from laminar to turbulent. The Archimedes number, calculated from the ratio of the Grashof number to the Reynolds number squared, is on the order of unity. These dimensionless numbers indicate that turbulence and buoyancy effects need to be included in the CFD model.

2.2. Room air flow model

2.2.1. Governing equations

The governing equations for air as an incompressible fluid using the standard $k-\varepsilon$ model are (in tensor notation) [17]:

(i) Mass conservation:

$$\frac{\partial u_i}{\partial x_i} = 0, \tag{1}$$

where u_i is the turbulent mean velocity in the x_i-direction.

(ii) Momentum conservation:

$$\rho \frac{\mathrm{D}u_i}{\mathrm{D}t} = -\frac{\partial p}{\partial x_i} + \frac{\partial (\tau_{ij})_{\mathrm{eff}}}{\partial x_j} + \rho_0(1-\beta\Delta T)g_i, \tag{2}$$

where ρ is the density, p is the pressure, ρ_0 is the density at a reference temperature T_0, ΔT is the temperature deviation from T_0, β is the coefficient of thermal expansion, g_i is the gravitational acceleration, and $(\tau_{ij})_{\mathrm{eff}}$ denotes the effective stress tensor given by

$$(\tau_{ij})_{\mathrm{eff}} = (\mu_{\mathrm{t}} + \mu)\left(\frac{\partial u_i}{\partial x_j} + \frac{\partial u_j}{\partial x_i}\right). \tag{3}$$

Here, μ is the molecular viscosity of air and μ_{t} is the eddy viscosity computed from

$$\mu_{\mathrm{t}} = \rho C_\mu \frac{k^2}{\varepsilon}, \tag{4}$$

where k is the turbulent kinetic energy, ε is the turbulent dissipation rate, and $C_\mu = 0.09$.

(iii) Energy conservation:

$$\rho c_{\mathrm{p}} \frac{\mathrm{D}T}{\mathrm{D}t} = \frac{\partial}{\partial x_j}\left[k_{\mathrm{eff}}\frac{\partial T}{\partial x_i} + u_i(\tau_{ij})_{\mathrm{eff}}\right], \tag{5}$$

where c_{p} is the specific heat, T is the temperature, and k_{eff} is the effective thermal conductivity, which, for the standard $k-\varepsilon$ turbulent model, is given by

$$k_{\mathrm{eff}} = k_{\mathrm{m}} + \frac{c_{\mathrm{p}}\mu_{\mathrm{t}}}{Pr_{\mathrm{t}}}. \tag{6}$$

Here, k_{m} is the molecular thermal conductivity, and Pr_{t} is the turbulent Prandtl number and equals 0.85.

(iv) Transport equations for k and ε:

$$\rho \frac{\mathrm{D}k}{\mathrm{D}t} = \frac{\partial}{\partial x_i}\left[\left(\mu + \frac{\mu_{\mathrm{t}}}{\sigma_{\mathrm{k}}}\right)\frac{\partial k}{\partial x_i}\right] + G_{\mathrm{k}} + G_{\mathrm{b}} - \rho\varepsilon \tag{7}$$

and

$$\rho \frac{\mathrm{D}\varepsilon}{\mathrm{D}t} = \frac{\partial}{\partial x_i}\left[\left(\mu + \frac{\mu_{\mathrm{t}}}{\sigma_\varepsilon}\right)\frac{\partial \varepsilon}{\partial x_i}\right] + C_{1\varepsilon}\frac{\varepsilon}{k}(G_{\mathrm{k}} + G_{\mathrm{b}}) - C_{2\varepsilon}\rho\frac{\varepsilon^2}{k}, \tag{8}$$

where G_{k} represents the generation of turbulent kinetic energy due to the mean velocity gradients and is written as

$$G_{\mathrm{k}} = \mu_{\mathrm{t}}\left(\frac{\partial u_i}{\partial x_j} + \frac{\partial u_j}{\partial x_i}\right)\frac{\partial u_i}{\partial x_j}. \tag{9}$$

G_{b} is the generation of turbulent kinetic energy due to buoyancy and is given by

$$G_{\mathrm{b}} = \beta g_i \frac{\mu_{\mathrm{t}}}{Pr_{\mathrm{t}}}\frac{\partial T}{\partial x_i}. \tag{10}$$

$C_{1\varepsilon}$ and $C_{2\varepsilon}$ are empirical constants, with values of $C_{1\varepsilon} = 1.44$ and $C_{2\varepsilon} = 1.92$. σ_k and σ_ε are turbulent Prandtl numbers for k and ε, with $\sigma_k = 1.0$ and $\sigma_\varepsilon = 1.3$.

(v) Near wall treatment:

When the mesh is such that the dimensionless length $y^+ \leqslant 11.225$ for cells adjacent to the wall, the laminar stress–strain relationship in terms of the dimensionless velocity U^+ is

$$U^+ = y^+. \tag{11}$$

The log-law is employed when $y^+ > 11.225$,

$$U^+ = \frac{1}{\kappa}\ln(Cy^+), \tag{12}$$

where

$$U^+ = \frac{\rho u_{\mathrm{p}} C_\mu^{1/4} k_{\mathrm{p}}^{1/2}}{\tau_{\mathrm{w}}} \tag{13}$$

and

$$y^+ = \frac{\rho C_\mu^{1/4} k_{\mathrm{p}}^{1/2} y_{\mathrm{p}}}{\mu}, \tag{14}$$

where κ is the von Karman constant and equals 0.42, C is an empirical constant equal to 9.81, u_{p} represents the turbulent mean velocity at point P tangential to the wall, k_{p} is the turbulent kinetic energy at point P, and y_{p} indicates the distance from point P to the wall.

(vi) Radiative transfer equation:

The radiative transfer equation for the radiant intensity I at position $\vec{r}$ in direction $\vec{s}$ of an absorbing, emitting, and scattering medium is

$$\frac{\mathrm{d}I(\vec{r},\vec{s})}{\mathrm{d}s} + (a_s + \sigma_s)\,I(\vec{r},\vec{s}) = a_s n^2 \frac{\sigma T^4}{\pi} + \frac{\sigma_s}{4\pi}\int_0^{4\pi} I(\vec{r},\vec{s}')\,\Phi(\vec{s}',\Omega')\,\mathrm{d}\Omega', \tag{15}$$

where s is the path length, a_s is the absorption coefficient, n is the refractive index, σ_s is the scattering coefficient, σ is the Stefan–Boltzmann constant, $\vec{s}'$ is the scattering direction vector, Φ is the scattering phase function, and Ω' is the solid angle. In the simulation, air is radiatively non-participating so that the absorption and scattering coefficients are zero.

The radiant intensity leaving a surface is given by

$$I = \frac{\varepsilon_s \sigma T^4}{\pi} + (1-\varepsilon_s)\int_{\vec{s}\cdot\vec{n}>0} I_{in}\vec{s}\cdot\vec{n}\,d\Omega, \tag{16}$$

where ε_s is the surface emittance, T is the surface temperature, I_{in} is the intensity of the irradiation, and $\vec{n}$ is the outward normal. The surfaces are gray, diffusely emitting and reflecting, and opaque. Polarization effects are absent. The net radiant flux leaving a surface is the difference between the emissive power and absorbed irradiation and is evaluated using

$$q''_r = \varepsilon_s \sigma T^4 - \varepsilon_s \int_{\vec{s}\cdot\vec{n}>0} I_{in}\vec{s}\cdot\vec{n}\,d\Omega. \tag{17}$$

2.2.2. Boundary conditions

The boundaries of the room are divided into 33 zones. Except for the inlets and outlet, all boundaries are wall boundaries. According to the location of the different surfaces, a wall boundary is assigned to one of three thermal boundary types, namely, adiabatic, constant temperature, and pseudo-convective boundary. All interior walls are adjacent to other rooms. There is a plenum above the ceiling and the floor is carpeted. Recognizing these conditions, the constant temperature assumption is made for all interior areas. The ledges on the outer sections of the exterior wall beneath the window are considered as adiabatic surfaces. For the three opaque sections of the exterior wall and the window, the pseudo-convective boundary condition is defined. An analysis is developed to account for heat transfer through the window and exterior wall when the overall conductance or U-value for the window or wall is specified. The overall heat flux q'' from the solution domain is defined by

$$q''_r = h_{ext}(T_0 - T_i) = h_f(T_i - T_f) + q''_r, \tag{18}$$

where T_i is the interior surface temperature of the wall or window, T_o is the exterior air temperature, h_{ext} is the pseudo-convective coefficient used by the solver for the temperature difference between T_o and T_i, h_f is the convective coefficient for the room air to the wall or window interior surface, T_f is the room air temperature near the surface, and q''_r is the internal radiative heat flux for a window or wall surface. For a general wall, the overall U-value, U_o is calculated according to [18]

$$U_o = \frac{1}{R_i + R_w + R_o}, \tag{19}$$

where R_i and R_o indicate interior- and exterior-side convective thermal resistances and R_w is the thermal resistance of the wall. Because the interior-side convective coefficient, R_i, is computed by the solver and radiant exchange is accounted for, the interior-side thermal resistance needs to be removed from the U-value in Eq. (19). The pseudo-convective coefficient used by the solver is then evaluated from

$$h_{ext} = \frac{1}{(1/U_0) - R_i}. \tag{20}$$

As previously noted, the exterior wall is divided into three sections, two side sections and a center section. The overall U-values for the three wall sections and the double pane window are used to describe the thermal communication between the interior surfaces and exterior environment for the east wall.

The supply air diffusers, as discussed in Section 2.3, are each divided into nine zones, with eight zones being open and a solid zone in the center as shown in Fig. 2. Different values and directions of the velocities are applied for zones 1–8. The inner ring represented by zones 1–4 has velocity V_1 and direction θ_1 and the outer ring described by zones 5–8 has velocity V_2 and θ_2. Values for V_1, θ_1 and V_2, θ_2 are the outputs of the diffuser model discussed in the next section. The velocity-inlet boundary condition is applied for the supply air diffusers. A uniform distribution of a variable, such as the velocity magnitude and direction, temperature, turbulent kinetic energy, and its dissipation rate, is used over each zone for each inlet. The turbulent kinetic energy of the discharge air from the supply air diffuser is estimated using [17]

$$k = \tfrac{3}{2}(u_{avg} I_t)^2, \tag{21}$$

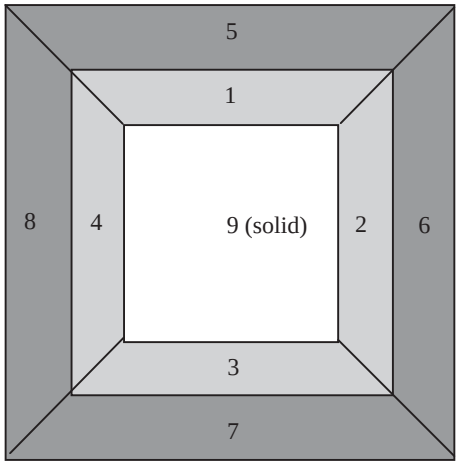

Fig. 2. Room diffuser plane view.

where u_{avg} is the average velocity magnitude of the discharge air and I_t is the turbulent intensity given by

$$I_t = \frac{u'}{u_{avg}} \cong 0.16(\mathrm{Re})^{-1/8}, \quad (22)$$

where the Reynolds number is determined by the discharge air velocity and the characteristic length $\sqrt[3]{XYZ}$. The turbulent kinetic energy dissipation rate at the diffuser outlet is calculated from

$$\varepsilon = C_\mu^{3/4} \frac{k^{3/2}}{I_t}. \quad (23)$$

The return air diffuser is defined as an out-flow boundary with unity weighting factor that implies that all supply air that comes in is exhausted at the return air diffuser.

2.3. Diffuser air flow model

To study the effects of the diffuser characteristics on the discharge air angles and air flow patterns in the near diffuser region, a diffuser model is configured. The room-side view of the square cone diffuser is shown in Fig. 3. Inspection of the actual air flow for the diffuser reveals that the air flow is mainly concentrated on the sides with very little air flow found at the corners. The picture in Fig. 3 illustrates that openings for the neck of the diffuser allow the supply air to flow out the sides. This air flow distribution differs from that for the diffusers investigated by Srebric and Chen [6], where a considerable amount of supply air discharges from the corners of a square cone diffuser. Recognizing that the air flow for the diffuser is concentrated on the sides and is symmetric with respect to the center plane, a 2-D model is developed.

The geometry for the 2-D CFD model is illustrated in Fig. 4a, which is built based upon information from the manufacturer and on-site measurements for the diffuser. The square cone type supply diffuser has a neck with a diameter of 0.25 m, an opening of $0.61 \times 0.61\ \mathrm{m}^2$, and is setup vertically by an offset of 0.05 m from the plane of the ceiling panels. The diffuser vanes are 45° to the ceiling plane and have horizontal projection lips that extend the vanes by about 0.025 m. When the offset is zero, the vanes lie below the ceiling plane, which is represented as dotted lines in Fig. 4a. The discharge angles of the inner and outer rings of the diffuser shown in Fig. 4b are defined as θ_1 and θ_2. The inlet of the neck is set as a uniform velocity inlet boundary condition [17] for the simulations, and the ceiling and diffuser vanes are treated as wall boundaries at a constant temperature. The dashed lines in Fig. 4a represent pressure outlet boundaries that maintain a constant pressure and allow outflow as well as inflow of air. The size of the 2-D flow domain has a width of 3.0 m and a depth of 1.2 m into the room.

Fig. 3. Geometry of square cone diffuser.

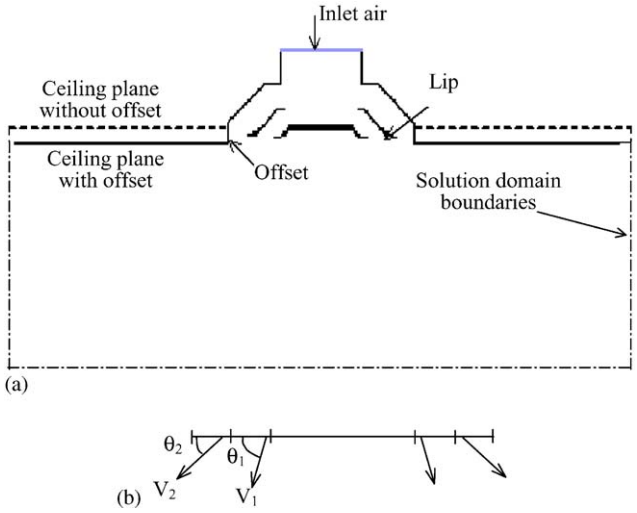

Fig. 4. Diffuser model: (a) 2D diffuser model; (b) sectional view of the diffuser.

For the 2-D diffuser air flow model, the governing equations for the air flow and heat transfer are the same as those listed previously for the 3-D room model, except that applying to a 2-D geometry and radiation exchange is not considered for the air flow in the diffuser. The inlet turbulent kinetic energy and its dissipation rate are calculated using the Reynolds number based on the velocity in the supply air duct and the diameter of the duct.

2.4. Numerical considerations

The governing equations for the room air flow are solved using the finite volume method with non-uniform, tetrahedral grids [17]. The air flow equations are solved using the SIMPLE algorithm [19]. The convective and diffusive terms are integrated using the

QUICK [20] difference scheme. The incomplete lower–upper decomposition method is used to solve the algebraic system. The radiant exchange relations are solved using the discrete transfer radiation method.

Each component of the room air flow model and the effects of grid size and convergence rates are assessed separately using previously documented problems with various geometries and boundary conditions. Air flow patterns in a cubic model room with one inlet centered on the ceiling and four outlets at the corners of the floor are examined for an isothermal condition. The results are compared with those of Murakami and Kato [21] and good agreement is found. The natural convection problem in a square cavity is simulated for Rayleigh numbers from 10^3 to 10^{12} and results for the air flow patterns and temperature distributions match well with those of Markatos and Pericleous [22]. A mixed-convection problem is examined to simulate a similar situation for the room. For this problem, the Nusselt numbers of the wall are of the same order of magnitude as those of Chen et al. [23]. The radiation model is solved for a 3-D rectangular enclosure and compared with results using the radiosity-irradiation method [24]. Good agreement is found for the radiant heat fluxes based on the model and the radiosity-irradiation method.

Mesh and initial condition independency are also examined. To choose an accurate as well as a computationally efficient mesh, a grid study showed that 462,582 tetrahedral elements non-uniformly distributed within the solution domain are needed for the room air flow model. Grids are very fine near diffusers and surfaces. The centers of the grids adjacent to each solid boundary for all boundaries are inside the viscous sublayer. The stretching factor, which is defined as the ratio of the succeeding grid interval versus the current grid interval, is controlled to be smaller than 1.14 for the mesh. For the 2-D diffuser model, a total of 27,000 uniformly distributed triangular elements are used. The initial values for k and ε need to be set smaller than the order of 0.01 to achieve converged criteria, which are set at 1×10^{-5} for the variables of pressure, velocity, temperature, k, and ε. The under-relaxation factors are adjusted downward when the residuals do not display smooth convergence.

As a means to evaluate the diffuser model, tests with low thermal mass screens and an infrared camera were used to visualize the air flow and to sense the air temperature. Cehlin et al. [15] reported that infrared pictures could provide an estimation of the air flow pattern and distribution from air supply diffusers. Previous studies [15,25,26] also indicated that solid and mesh type screens made of a dielectric material (paper or fiberglass) work best. In the tests, three screens, namely, a charcoal-color fiber net (with an opening of 70%), a clear vinyl sheet, and an opaque brown paper sheet, were considered. Each screen with the dimensions of at least $1.2 \times 1.8\,\mathrm{m}^2$ was hung perpendicular to the ceiling, in an east–west orientation, and centered beneath the east supply air diffuser of the room as shown in Fig. 5. The infrared camera was held 2 m away from the center of the diffuser with the sensing element parallel to the screen. The temperature of the discharge air was varied from 286 to 305 K and the supply air volumetric flow ranged from $Q = 0.09$ to $0.47\,\mathrm{m}^3/\mathrm{s}$. The infrared pictures were taken when the system was at near steady-state conditions. The results indicate that the infrared pictures for the fiber net and vinyl screens displayed conditions behind the screen (screens are partially transparent) and do not properly represent the temperature of the screen. The paper screen provides the best indication of the air flow and temperature distributions.

Fig. 5. Screen setup.

Although no comparisons are reported for air flow in the room, the results from several of the selected numerical problems previously discussed under numerical assessment have been compared by the authors of the studies to experimental results. Hence, there is a certain level of confidence that the solver, with the stated governing equations, boundary conditions, and numerical procedures, produces representative results.

3. Results and discussions

3.1. Diffuser characteristics

The influences of diffuser offset and lips on the air flow direction are examined using the 2-D diffuser model with and without an offset (WO, NO) and lips (WL, NL). The ceiling and diffuser walls are set at a constant temperature of 294 K and the surrounding air has an initial temperature of 294 K. The size of the solution domain, $3.0 \times 1.2\,\mathrm{m}^2$, is sufficiently large so that the out-flow boundaries do not affect the air flow field in the vicinity of the diffuser. The gravitational acceleration is $9.81\,\mathrm{m/s}^2$.

As shown later, the temperature distributions are representative of the air flow pattern and, therefore, are only reported for the diffuser results. The temperature distributions in half of the solution domain with $Q = 0.14\,m^3/s$ and an inlet temperature of 286 K (cooling case) are shown in Fig. 6. As a point of reference, the minimum outdoor air flow recommended assuming two people in the room of the stated size is $0.028\,m^3/s$ [18], which is $0.014\,m^3/s$ for one diffuser. The actual air flow is larger to account for ventilating and conditioning of the room and is commonly found when conventional control schemes are used [16]. The results for the NO cases show that the lip projections have the effect of directing the cold air along the ceiling when compared to NO/NL and NO/WL cases. When the NO and WO cases are compared, the offset forces the air flow to be directed downward to the lower part of the room. Also, in the presence of an offset, the temperature distribution around the diffuser becomes independent of the lips for the cooling cases.

The temperature distributions for an inlet temperature of 305 K (heating case) are shown in Fig. 7. Results indicate that buoyancy causes the warm air to flow along the ceiling when an offset is absent. The diffuser lips enhance the buoyancy effect and cause warm air to attach to the ceiling. When an offset exists, the lips direct more of the supply air along the vertical offset, which causes the warm air to flow downward as illustrated by the WO/WL case when compared to the WO/NL case.

The offset and lips of the diffuser work together to determine the air flow patterns in the near diffuser region. The presence of an offset does not change the actual opening area for each diffuser but affects the velocity distribution across different zones. For the cases when the diffuser lips exist, the total effective flow area is reduced which results in an increase in the velocity magnitude. The angles and average velocity magnitude for the discharge air in each zone corresponding to the cases in Figs. 6 and 7 are listed in Table 1. A value of $\theta_1 = 0^\circ$ deg implies that the air flows along the ceiling and occurs when the offset is absent. The cases when lips are present (WL) either with or without the offset have discharge angles that are independent of the supply air temperature. An inspection of the velocity magnitude at discharge shows that, for both cooling and heating cases, the average discharge velocity of the inner ring, V_1, is higher by about 5% of that for the outer ring, V_2. Based on these findings, it is appropriate to assume that, for the considered conditions, the velocity magnitude is uniform for the different zones of the diffuser.

The temperature distributions using infrared visualization and CFD simulation for the WO/WL case with the same air flow and temperature conditions are

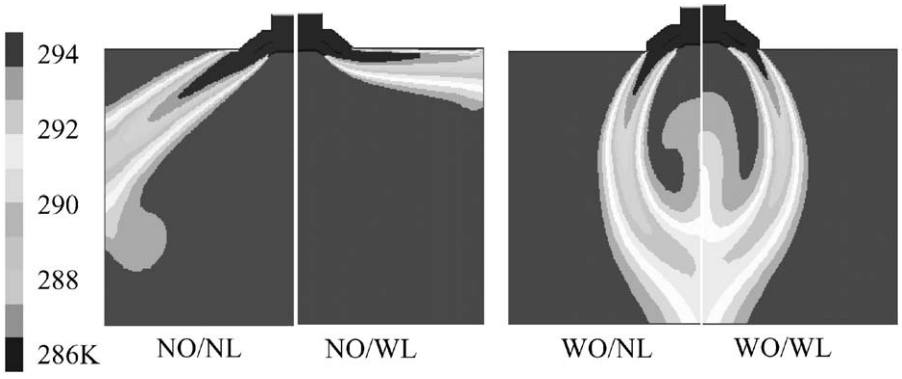

Fig. 6. Temperature distributions for cooling case.

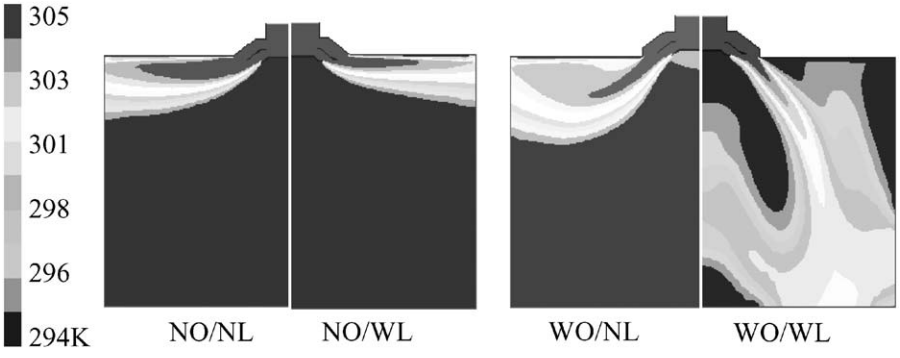

Fig. 7. Temperature distributions for heating case.

Table 1
Supply air discharge velocity magnitudes and angles

Geometry	Cooling				Heating			
	V_1 (m/s)	V_2 (m/s)	θ_1 (°)	θ_2 (°)	V_1 (m/s)	V_2 (m/s)	θ_1 (°)	θ_2 (°)
NO/NL	0.51	0.49	45	30	0.50	0.50	30	0
NO/WL	0.52	0.51	30	0	0.52	0.52	30	0
WO/NL	0.51	0.49	60	45	0.51	0.50	75	60
WO/WL	0.52	0.51	75	60	0.52	0.51	75	60

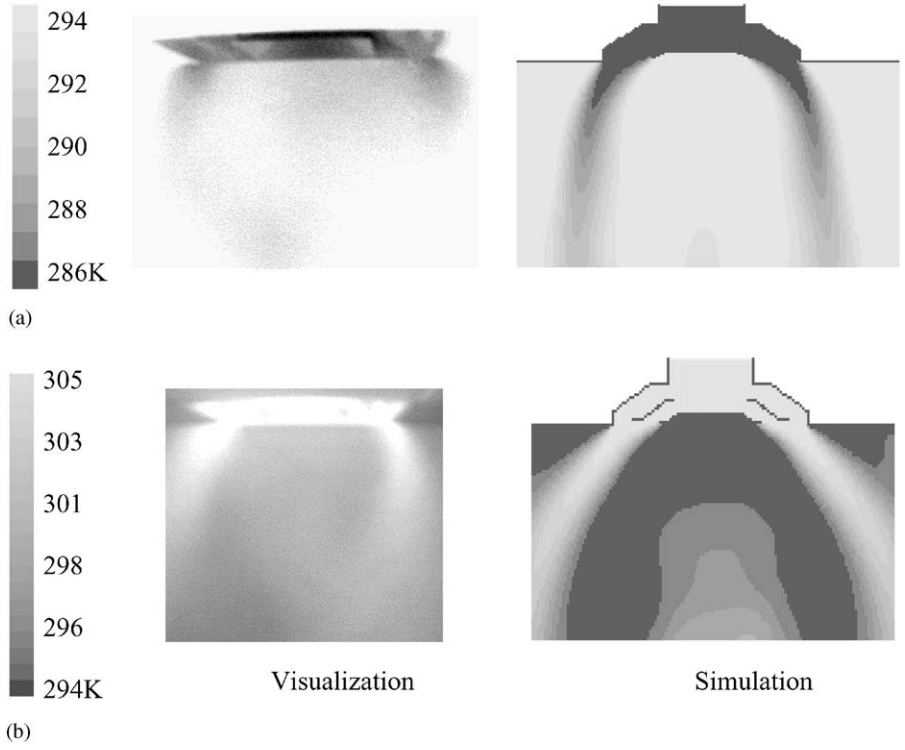

Fig. 8. Comparison of infrared visualizations and simulation results: (a) temperature distributions for cooling case WO/WL; (b) temperature distributions for heating case WO/WL.

displayed side-by-side in Fig. 8. For the cooling case, as shown in Fig. 8a, the darkened regions indicate the cold air stream that has similar discharge angles as those for the results from the simulation. Fig. 8b demonstrates the heating case where the brightened regions denote warm inlet air. Although the resolution of the infrared pictures is fairly low, the air flow patterns indicated in the pictures still show that the simulation results provide an acceptable representation of the air flow temperatures displayed by the infrared camera. Because of the busy test schedules at the test facility [16], comparisons for other conditions and diffuser geometries were not possible.

To further study the air flow characteristics of the diffuser, the effect of buoyancy versus momentum is examined by choosing different supply air flows without changing other conditions. Results for the heating condition, where the inlet air temperature is 305 K, are examined in Fig. 9. For the WO/WL case with $Q = 0.1\,m^3/s$ in Fig. 9a, buoyancy causes the air to flow along the ceiling. At supply air flows of 0.14 and $0.23\,m^3/s$ as illustrated in Figs. 9b and c, the larger discharge air angles indicate that the air flows downward to the lower part of the room. The relation between the momentum and buoyancy terms, which can be evaluated by the Archimedes number, determines the air flow pattern of the room. For three cases considered in Fig. 9, the ratios for Archimedes numbers (Ar) of the different cases are, $Ar_1/Ar_2 = 2.25$ and $Ar_1/Ar_3 = 6.25$, where subscripts of 1, 2, and 3 refer to the respective air flows. With the increase of air flow, the buoyancy term is still the same but the momentum term increases. When

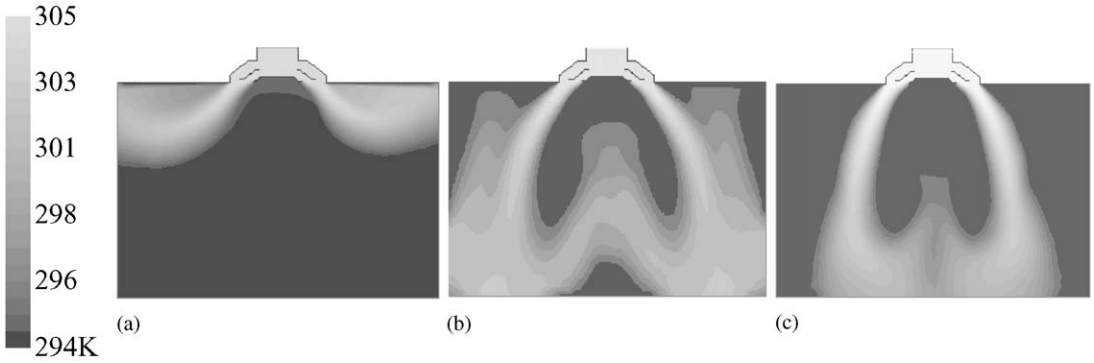

Fig. 9. Temperature distributions for different air flows for heating WO/WL case: (a) $Q = 0.10\,m^3/s$, (b) $Q = 0.14\,m^3/s$, (c) $Q = 0.23\,m^3/s$.

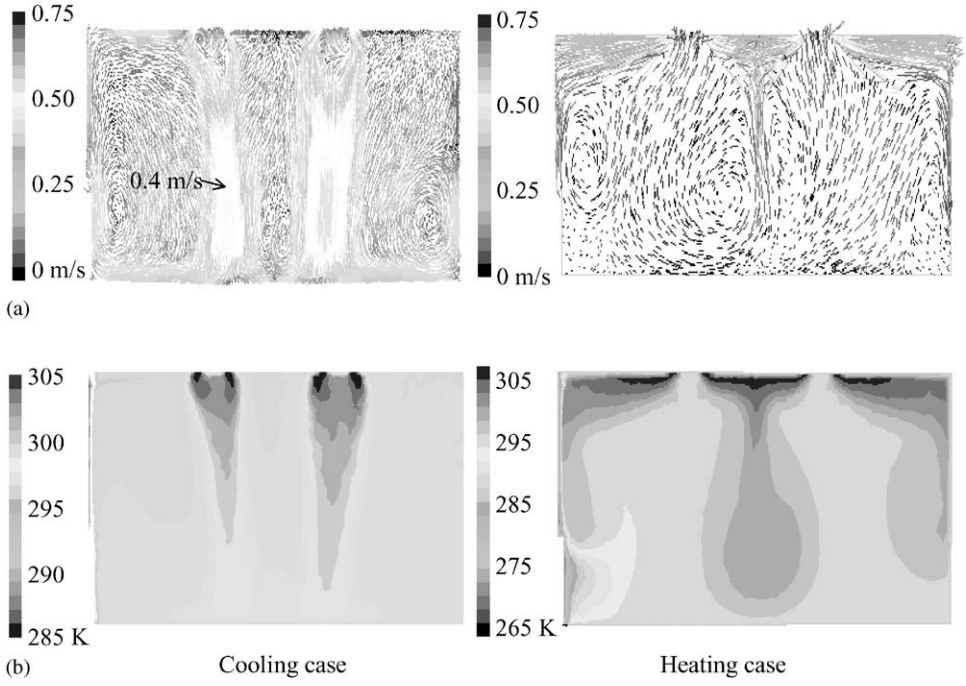

Fig. 10. Air flow and temperature distributions for A–A plane: (a) air flow patterns; (b) temperature distributions. (Gray scales in flow patterns indicate magnitude of velocity vectors).

the supply air velocity is low, the air jet is attached to and flows along the ceiling (Fig. 9a) due to the Coanda effect [27].

3.2. Room heating and cooling

The discharge air angles and velocities determined from the 2-D diffuser model for the WO/WL case were implemented in the 3-D room model to study the air flow pattern and temperature distribution in the room. There are no internal heat sinks/sources inside the room. Simulations were conducted for both cooling ($T_o = 308\,K$) and heating ($T_o = 255\,K$) of the room. The summer and winter overall U-values are 0.44 and $0.43\,W/m^2\,K$ for the wall side sections, 0.83 and $0.85\,W/m^2\,K$ for the wall center section, and 0.32 and $0.37\,W/m^2\,K$ for the window. The air flow per diffuser is $0.14\,m^3/s$, which corresponds to an average discharge velocity of 0.5 m/s, and the discharge air angles are $\theta_1 = 75^\circ$ and $\theta_2 = 60^\circ$. As shown in Table 1, the discharge angles for the WO/WL case are independent of the supply air temperature. With the exception of the east wall and window, the remaining walls of the room are at a temperature of 294 K. Air flow patterns and temperature distributions for the WO/WL, cooling and heating cases in the room center plane right across two supply air diffusers for plane A–A in Fig. 1 ($Y = 2.29\,m$) are shown in Fig. 10. The window is on the left. The air flow patterns are represented using lines whose lengths indicate the magnitude of the velocity vector at a

particular point in the room. In some plots, the lines extend beyond the boundaries but this does not imply that there is air flow across a boundary.

For the cooling case, the air streams from a diffuser merge together below each diffuser to form two jets, and the buoyancy force carries the cold air down to the floor with only a small decrease in the air velocity. For this case, people in the occupied zone, which is usually defined as a region within 1.8 m of the floor and 0.3 m away from the walls, will feel a strong air stream blowing on them, thereby causing a draft. It is recommended [18] that the velocity should be less than 0.25 m/s for occupant comfort, however, the maximum velocity in the occupied region for this case is around 0.4 m/s. A small portion of the air flows to the center of the room, but most of the air flows outward to the vertical walls. When the cold air hits the vertical walls, especially the warm window, it is warmed and begins to travel upwards. Two vortices form in the corners of the floor and a vertical wall. The mean air temperature of the room is 294 K and the surface temperature of the window is 303 K in the absence of the radiant exchange. Due to the buoyancy effect, the heated air near the window flows upwards and blends with the incoming cold air jet from the supply diffuser.

As shown in Fig. 10, the Coanda effect exists for the heating case. The buoyancy force causes the warm air to flow along the ceiling, where some of the inlet air flows directly to the outlet without mixing with the room air as shown in Fig. 11, where the flow patterns for plane B–B across the east supply diffuser and the return grill are shown. This direct return of the inlet air could lead to a waste of energy. The remaining supply air flows down along the window and west wall to the floor. With the air flowing along a vertical wall, the air velocity dissipates. In the center of the room, two inlet air streams merge together into a single stream that flows downward to the floor and a warm region is produced near the center of the room. The temperature distribution for the heating case is opposite to the cooling case

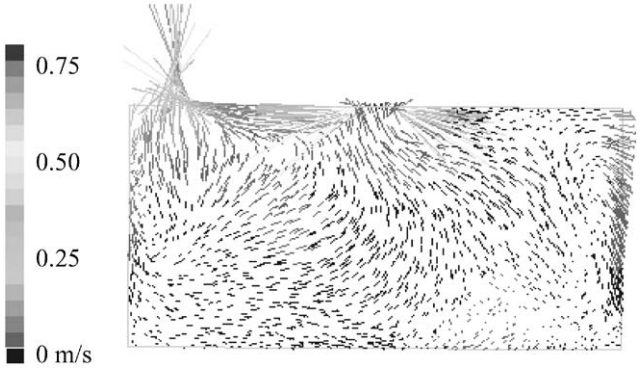

Fig. 11. Air flow pattern at B–B plane for heating case (gray scales in flow patterns indicate magnitude of velocity vectors).

Table 2
Results for the exterior window with and without radiation[a]

Case	Variable	Cooling	Heating
Without radiation	q''_w (W/m^2)	17.8	53.8
	T_w (K)	303.4	271.1
With radiation	q''_w (W/m^2)	38.8	93.2
	T_w (K)	299.6	279.6

[a]Results from simulations.

with the warm air near the ceiling and a cold region below the window. The mean air temperature of the room for the heating case is 294 K and the surface temperature for the window without radiation is 271 K. Because the window acts as a heat sink, the temperature of the warm air coming from the ceiling decreases as it flows past the window. Due to buoyancy, a portion of the low temperature air accumulates on the window bay and creates a strong cold air draft below the window. This cold air flows downward from the window with a velocity of around 0.3 m/s and a temperature of 290 K.

The effect of the radiant exchange between the surfaces of the room is now taken into account. The results indicate that the radiant exchange does not have a significant influence on the air flow patterns and temperature distributions within the room. The radiant exchange between the window and the interior surfaces, however, does affect the heat flux for the window. Results for the window heat fluxes and average window temperatures for the cooling and heating cases with and without radiation being accounted for are illustrated in Table 2. The results for the heat fluxes indicate that the heat flux with radiation is about twice that when radiant exchange is neglected. When radiation is considered, the temperature of the window is decreased by 4 K for the cooling case and is increased by 8 K for the heating case. The decrease (increase) of the window temperature for the cooling (heating) case is because of the radiant exchange with the walls of the room, which are at 294 K.

3.3. Single diffuser

The results thus far are for two air supply diffusers. In some applications and to reduce the nonuniformities of the temperature distributions in a room, a single diffuser is used. The effect of having one diffuser is examined by considering that the east-most diffuser is active and the west diffuser (WO/WL) is not operating. The 2-D diffuser model was executed for the cooling and heating cases for an air flow of 0.28 m^3/s and the results are displayed in Fig. 12. The temperature distributions show that the air has a strong vertical downward flow that is independent of whether the air is cooled or heated relative to the temperature of the surrounding air. The values for the air flow discharge angles are nearly

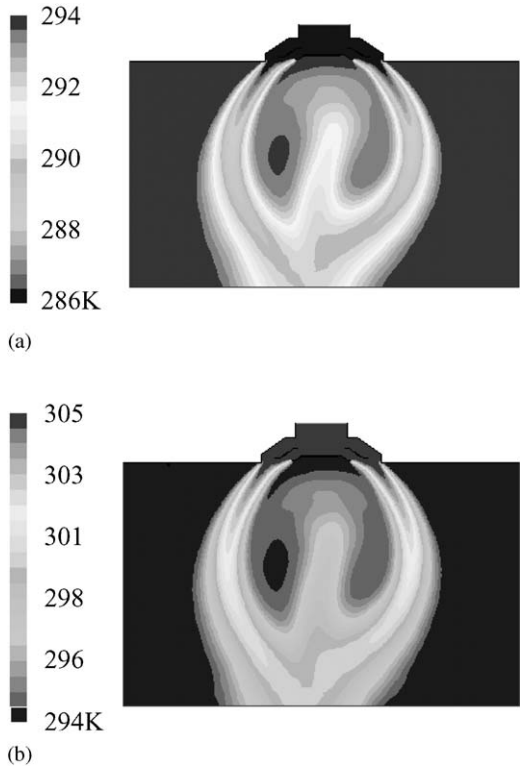

Fig. 12. Temperature distributions for a single diffuser: (a) cooling case for $Q = 0.28\,m^3/s$: $\theta_1 = 75°$, $\theta_1 = 60°$; (b) heating case for $Q = 0.28\,m^3/s$: $\theta_1 = 75°$, $\theta_1 = 60°$.

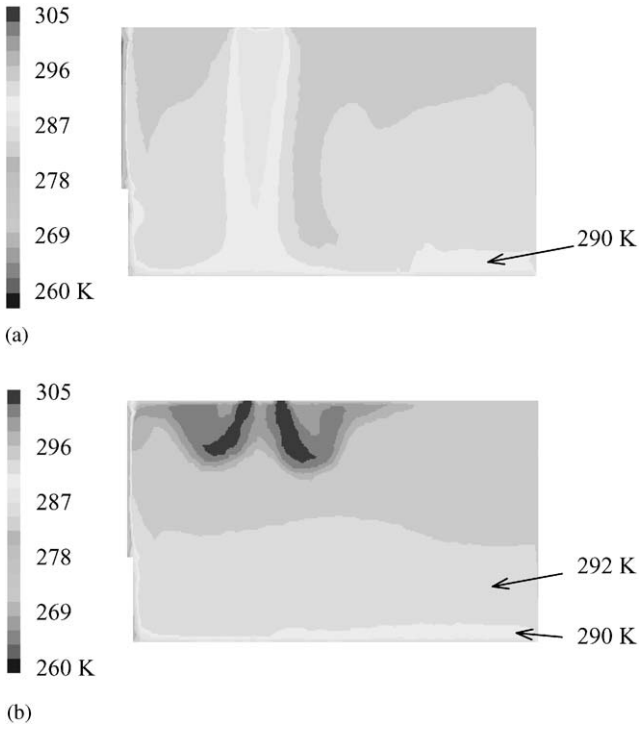

Fig. 13. Temperature distributions at A–A plane for a single diffuser: (a) Heating case; (b) cooling case.

independent of the supply air temperature and have values of $\theta_1 = 75°$ and $\theta_2 = 60°$. The magnitudes of the mean velocities of the discharge air are almost the same for each zone, which implies that $V_1 = V_2 = 1\,m/s$.

The air flow characteristics of the room with a single supply diffuser are examined using the discharge angles determined from the diffuser model. The results for the room model indicate that the air flow patterns are adequately described by the temperature distributions; therefore, Fig. 13 only presents temperature distributions at A–A plane for the cooling and heating cases. For comparison purposes, the temperature scales for the cooling and heating cases are identical. For the cooling case shown in Fig. 13a, the air flows downward, strikes the floor, and then is distributed throughout the room. The comparison between Figs. 10 and 13 shows that more mixing occurs for the case of a single diffuser than for two diffusers. For a horizontal plane near the vertical center of the room, the temperature varies from 286 to 294 K, where the coldest temperature is due to the supply air jet. The temperature near the bottom of the room is about 290 K.

The temperature distribution for the heating case is shown in Fig. 13b, where the cold window is seen on the left. The temperatures in Fig. 13b indicate that, after the air is injected into the room, it turns upward and flows along the ceiling and cools rapidly. The jets from the diffuser penetrate deeper into the room than when two diffusers are used. The temperature of the room is stratified into three layers, the upper layer, the intermediate layer at a temperature of 292 K, and a narrow layer at the bottom with a temperature of 290 K. Because the warm air coming from the ceiling has larger momentum than that for the case for two diffusers, the cold window has a smaller effect on the incoming air stream and, therefore, does not result in a cold region beneath the window as seen in Fig. 10. The results using a single diffuser show better uniformity of the room air temperature than that for two diffusers.

4. Conclusions

The CFD models for a supply air diffuser and a room are developed to examine the effects of various factors on the air flow patterns and temperature distributions. Simulations are conducted for different indoor and outdoor conditions to account for heating and cooling of the room. Results from the 2-D diffuser model show that the offset and lips of the diffuser determine the discharge air angle and air flow patterns in the near diffuser region. The air discharge angles for the WO/WL case show good agreement with those observed from infrared photos. Buoyancy plays an important role in determining the room air flow patterns. For small discharge angles of the heating case, due to the Coanda

effect, the air jets flow along the ceiling. The radiant exchange between the window and interior surfaces contributes about one-half of the total heat transfer for the window for both summer and winter and also causes a significant change in the window temperature. The comparison between operating two diffusers and a single diffuser at the same air flow shows a better uniformity of room air temperature for the case of only one diffuser.

The results obtained from this study can be used to improve the design of the supply air devices and the layout of the supply and return air diffusers in a conditioned room. A better understanding for the air flow characteristics of a room helps to develop simulation tools for the purpose of examining energy efficient operating strategies and control algorithms.

Acknowledgements

This study was made possible through Grant No. 96-10a from the Iowa Energy Center. The authors thank Prof. Ching-Long Lin of The University of Iowa for his contribution to this study.

References

[1] Chen Q, Srebric J. A procedure for verification, validation, and reporting of indoor environment CFD analyses. HVAC&R Research 2002;9(2):201–16.
[2] Heikkinen J. Modeling of a supply air terminal for room airflow simulation. In: Proceedings of the 12th AIVC conference, vol. 3, Ottawa, Canada, 1991. p. 213–26.
[3] Chen Q, Moser J. Simulation of a multiple-nozzle diffuser. In: Proceedings of the 12th AIVC conference, vol. 2, Ottawa, Canada, 1991. p. 1–14.
[4] Djunaedy E, Cheong KWD. Development of a simplified technique of modeling four-way ceiling air supply diffuser. Building and Environment 2002;37(4):393–403.
[5] Nielsen PV. Description of supply openings in numerical models for room air distribution. ASHRAE Transactions 1992;98(1): 963–71.
[6] Srebric J, Chen Q. Simplified numerical models for complex air supply diffusers. HVAC&R Research 2002;8(3):277–94.
[7] Launder BE, Spalding DB. The numerical computation of turbulent flows. Computer Methods in Applied Mechanics and Engineering 1974;3(2):269–89.
[8] Murakami S, Ohira N, Kato S. CFD analysis of a thermal plume and the indoor air flow using k–ε models with buoyancy effects. Flow, Turbulence and Combustion 2000;63(1):113–34.
[9] Sinha SL, Arora RC, Roy S. Numerical simulation of two-dimensional room air with and without flow. Energy and Buildings 2000;32(1):121–9.
[10] Gan G, Awbi HB. Numerical simulation of the indoor environment. Building and Environment 1994;29(4):449–59.
[11] Rees SJ, McGuirk JJ, Haves P. Numerical investigation of transient buoyancy flow in a room with a displacement ventilation and chilled ceiling system. International Journal of Heat and Mass Transfer 2001;44(16):3067–80.
[12] Chow WK. Numerical studies of airflows induced by mechanical ventilation and air-conditioning. Applied Energy 2001;68(2): 135–59.
[13] Posner J, Buchanan C, Dunn-Rankin D. Measurement and prediction of indoor air flow in a model room. Energy and Buildings 2003;35(5):515–26.
[14] Zhao L, Zhang Y, Wang X, Riskowski GL, Christianson LL, Chen Q. Measurement of two-dimensional air velocities in a full-scale room using particle image velocimetry. ASHRAE Transactions 2001;107(2):434–44.
[15] Cehlin M, Moshfegh B, Sandberg M. Measurements of air temperatures close to a low-velocity diffuser in displacement ventilation using an infrared camera. Energy and Buildings 2002;34(7):687–98.
[16] IEC, http://www.energy.iastate.edu/ers/, Iowa Energy Center, 2003.
[17] Fluent, Fluent 5.5.14 manual, Fluent, Inc., 1999.
[18] ASHRAE. ASHRAE handbook of fundamentals. American Society of Heating, Refrigerating, and Air-Conditioning Engineers, Inc., 2001.
[19] Patankar SV. Numerical heat transfer and fluid flow. New York: McGraw-Hill; 1980.
[20] Leonard BP. A stable and accurate convection modeling procedure based on quadratic upstream interpolation. Computer Methods in Applied Mechanics and Engineering 1979;19(1): 59–98.
[21] Murakami S, Kato S. Numerical and experimental study on room airflow—3-D predictions using k–ε turbulent model. Building and Environment 1989;24(1):85–97.
[22] Markatos NC, Pericleous KA. Laminar and turbulent natural convection in an enclosed cavity. International Journal of Heat and Mass Transfer 1984;27(5):755–72.
[23] Chen TS, Armaly BF, Ramachandran N. Correlations for laminar mixed convection flows on vertical, inclined, and horizontal flat plates. Journal of Heat Transfer 1986;108(4): 835–40.
[24] Ehlert JR, Smith TF. Surface radiation for three-dimensional rectangular enclosures using the discrete-ordinates method. Journal of Thermophysics and Heat Transfer 1994;8(3):628–31.
[25] Sundberg J. Use of thermography to register air temperatures in cross-sections of room and to visualize the air flow from air supply diffusers. In: Proceedings of thermosense XV, vol. 1933, Florida: SPIE; 1993. p. 61–6.
[26] Hassani VA, Stetz M. Application of infrared thermography to room air temperature measurements. ASHRAE Transactions 1994;100(2):1238–47.
[27] Graebel WP. Engineering fluid mechanics. New York: Taylor & Francis; 2001.